Sedimentology (2007) **54,** 1–17 doi: 10.1111/j.1365-3091.2006.00816.x

Geochemical and Nd isotope composition of detrital sediments on the north margin of the South China Sea: provenance and tectonic implications

YI YAN*, BIN XIA*, GE LIN*, ANDY CARTER†, XIAOQIONG HU*, XUEJUN CUI*, BAOMING LIU*, PIN YAN* and ZHENGJIANG SONG‡
*Key Laboratory of Marginal Sea Geology, Guangzhou Institute of Geochemistry, Chinese Academy of Sciences, Wushan, Guangzhou 510640, China (E-mail: yanyi@gig.ac.cn)
†Research School of Earth Sciences, University and Birkbeck College, Gower Street, London WC1E 6BT, UK
‡Daqing Oilfield Company Limited, Daqing 163311, China

ABSTRACT

A major re-organization of regional drainages in eastern Tibet and south-western China took place in the Cenozoic as deformation from the growing Himalayas and Tibetan Plateau affected an increasingly wider area. The effects of these changes on the regional sediment routing systems is not well constrained. This study examines the geochemical and Nd signatures of sedimentary rocks from the Ying-Qiong and Nanxiong basins on the northern margin of the South China Sea to constrain and identify any significant changes in sediment source. Upper Cretaceous to Lower Eocene sedimentary rocks in the Nanxiong Basin show higher Th/Sc, La/Sc, Th/Cr and Th/Co ratios and lower Eu/Eu* ratios than PAAS (post-Archaean Australian Shale), which indicates that Palaeozoic sedimentary rocks of the South China Block were the main basin sediment source. In contrast, Oligocene to Pleistocene sedimentary rocks of the Ying-Qiong Basin show an abrupt change in these trace-element ratios between 16·3 and 10·4 Ma, indicating a mid-Miocene shift in provenance. ε_{Nd} values from the Ying-Qiong Basin (range = −11·1 to −2·1) reinforce this, with pre-13·8 Ma sedimentary rocks having average ε_{Nd} of −5·6 (range = −2·1 to −7·4), and post-13·8 Ma sedimentary rocks having average ε_{Nd} of −9·3 (range = −8·7 to −11·1). During the Oligocene, the centre of rifting transferred south and basins on the north margin of the South China Sea experienced rapid subsidence. Further uplift and erosion then exposed Mesozoic and Cenozoic granites that supplied large amounts of granitic detritus, especially to the Ying-Qiong Basin. Then a change occurred at *ca* 13 Ma resulting in less input from local sources (i.e. the fault blocks formed by Mesozoic-Cenozoic tectonics and magmatism) to an increasing contribution of older continental material, mostly from Indochina to the west of the South China Sea.

Keywords Basins; geochemistry; Nd isotope; provenance; South China Sea.

INTRODUCTION

Geochemical signatures of sediments deposited on passive margins provide important sources of information that record the evolving provenance, tectonic, environmental and ecological evolution of margin and hinterland (Clift *et al.*, 2002; Li *et al.*, 2003). Although processes such as weathering, erosion, sedimentation and diagenesis can alter the geochemical composition of basin sediments, there often remains a strong signature of the original source terrain (Roser & Korsch, 1988;

McLennan & Taylor, 1991). Significant improvements in analytical precision and approaches to monitoring sediment geochemistry, especially through the introduction of discrimination diagrams based on the relationship of selected major and trace elements (Roser & Korsch, 1986; Condie, 1993; Cullers, 1994) have advanced the ability to extract this source information. The distribution of selected trace elements, such as rare earth elements (REEs) (e.g. Y, Sc, Th, Zr, Hf, Cr and Co), is a useful indicator of source region composition and tectonic setting because they are generally immobile and retain their original ratios during the process of erosion, transport and deposition (Taylor & McLennan, 1985).

Similarly, Sm-Nd isotope studies have been shown to be a powerful tool for investigating the sources of sedimentary rocks because Nd isotopic composition is related to the age of terrane source rocks (Biscaye *et al.*, 1974; Goldstein *et al.*, 1984; Grousset *et al.*, 1988) and is largely unaffected by processes of weathering, erosion and deposition (e.g. Clauer & Chaudhuri, 1992; Li *et al.*, 2003). Neodymium isotopic studies of shale are now widely used to determine the average age and composition of the eroded source continental crust and, subsequently, to determine rates of continental growth (Jacobsen, 1988). In this study trace element and Nd isotope signatures are analysed to investigate the provenance of sediments deposited in South China Sea basins.

Across SE-Asia the Cenozoic is noteworthy as an era of major tectonic activity that impacted on landform development, climate and biology (Dewey *et al.*, 1989; Rowley, 1996; Najman & Garzanti, 2000). At the heart of this change is the collision of India with Eurasia, closure of the Tethyan Ocean (Wang *et al.*, 2002) and formation of the Himalayas and Tibetan Plateau through crustal shortening and thickening (Houseman & England, 1996). Soon after, the South China Sea began to develop, and although intrinsically linked to the India–Asia collision, the precise mechanism for rifting and spreading is hotly debated (e.g. England & Houseman, 1986; Leloup *et al.*, 1995; Lacassin *et al.*, 1997). For this reason a great deal of research effort has been directed at the structural and tectonic development of the South China Sea (Ru & Pigott, 1986; Rangin *et al.*, 1995; Yan *et al.*, 2001) largely to the neglect of its sediment record.

In the Late Mesozoic and Cenozoic, uplift of the South China Block (Zou, 1995), coincided with deposition of considerable thickness of sediment in basins along the northern margin of the South China Sea including the Nanxiong Basin, the Pearl River Mouth Basin, and the Ying-Qiong Basin (Fig. 1). The relationship between uplift and basin sedimentation would seem straightforward with the bulk of sediment presumed to have been sourced from the uplifted South China Block. However recent Nd-isotopic analysis of sediment at Ocean Drilling Program (ODP) Site 1148 (18°50·17′ N, 116°33·94′ E) suggested that pre-27 Ma sedimentary rocks were mainly derived from a region to the south-west, whereas post-23 Ma sedimentary rocks were derived from the north consistent with the South China Block (Li *et al.*, 2003). Furthermore, geomorphic studies in eastern Tibet suggest that the regional drainage system changed throughout the Cenozoic as the Tibetan Plateau uplifted (Clark *et al.*, 2005). Such changes would have affected sediment source and delivery into South China Sea basins. To investigate the extent of South China Block and/or Tibetan Plateau contributions to sedimentation in basins along the north margin of the South China Sea, this study examined the trace element and Nd isotopic compositions of sedimentary rocks collected from the Nanxiong and Ying-Qiong basins.

GEOLOGICAL SETTING

The bulk of the South China Block is Proterozoic-Late Archaean (Ames *et al.*, 1996) formed of mainly low-grade clastic metasediments with minor volcanic rocks (Li & McCulloch, 1996) and a non-metamorphic shelf to continental sequence that spans the Neoproterozoic to Triassic. From the Late Triassic onwards, sedimentation on the South China Block was dominated by continental red beds (Ling *et al.*, 1996; Chen & Jahn, 1998). During the Late Jurassic to Cretaceous the region was an active Andean-type magmatic arc subject to block faulting (Xu, 1990) and granite emplacement (Zou, 1995).

From the Late Cretaceous onwards, many small rifts developed during three main phases of rifting including the Nanxiong Basin and the Ying-Qiong Basin. The first episode of rifting started in the Late Cretaceous and ended in the Early Eocene (from *ca* 96 to 50 Ma). Largely centred on the South Chian Block this event formed numerous small rifts along NE-trending faults. Sedimentation was mainly fluvial-lacustrine red beds. The second rifting episode, centred to the south of the first phase, took place in the Middle Eocene and ended in the Early

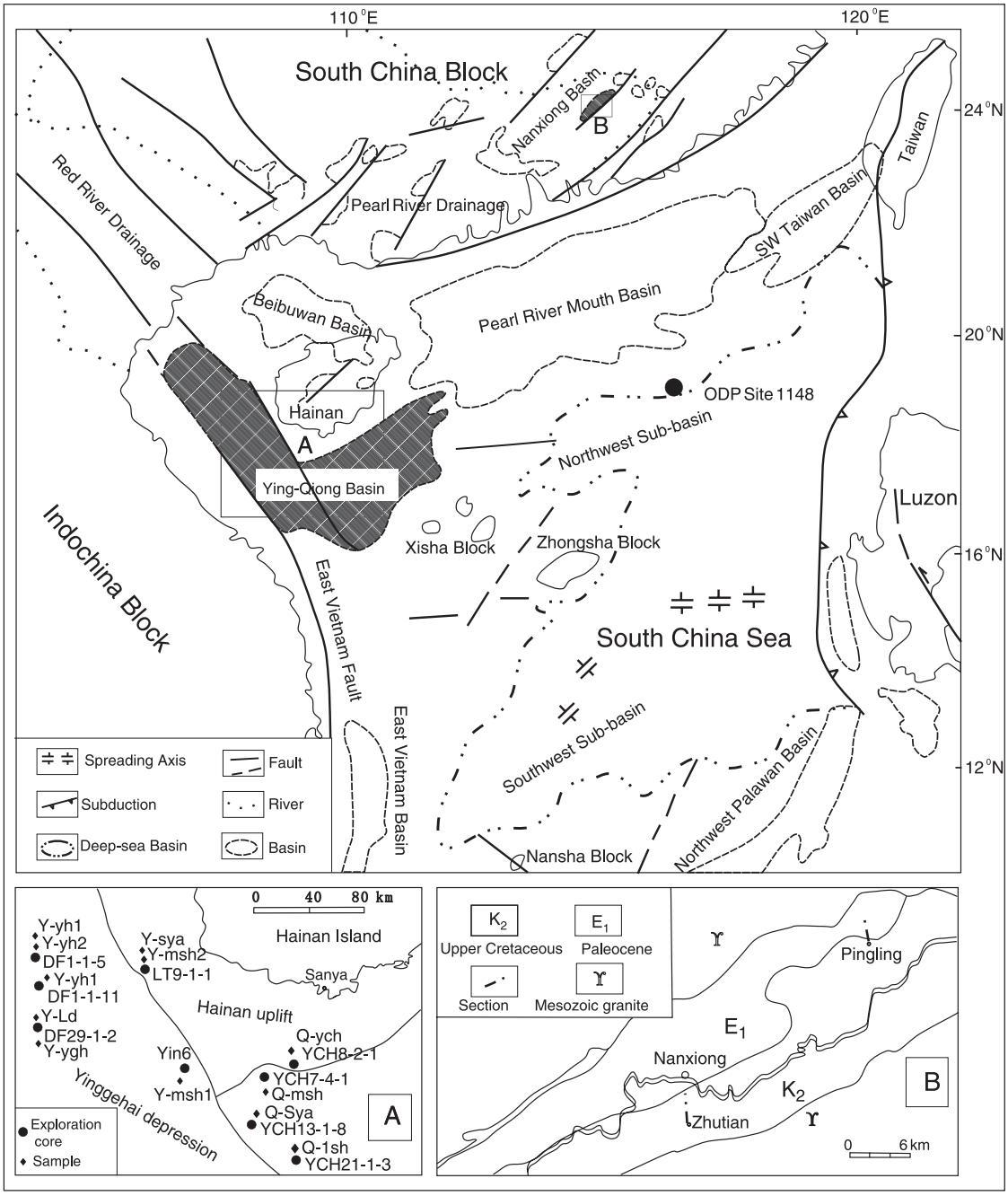

Fig. 1. Tectonic setting of the north margin of the South China Sea (modified after Zhou *et al.*, 1995); (A) Location of samples from the Ying-Qiong Basin; (B) location of samples from the Nanxiong Basin.

Oligocene (from *ca* 50 to 29·3 Ma). Basins on the north margin of the South China Sea experienced rapid subsidence and in the Ying-Qiong Basin sedimentation was dominantly coarse-grained fluvial with restricted lacustrine facies (Ru & Pigott, 1986; Gong & Li, 1997). The third and final stage of rifting occurred in the Late Oligocene (from *ca* 29·3 to 23·3 Ma), and is associated with alternating marine and terrestrial sequences characterized by coarse-grained clastic sediments. Post-rift thermal subsidence, from *ca* 23·3 Ma to the present and a regional transgression led to deposition of hemipelagic marine sediments in the Ying-Qiong Basin (Zhou *et al.*, 1995). This basin also experienced two further rapid subsidence events during the Early-Middle Miocene and Pliocene, associated with wrench motion along the Red River Fault (Sun *et al.*, 1995).

SAMPLE DESCRIPTION AND ANALYTICAL TECHNIQUES

Samples were collected from the exploration cores in the Ying-Qiong Basin and from outcrops in the Nanxiong Basin (Figs 1 and 2) that together provide a record of erosion from the Late Cretaceous to the Pleistocene. Most of the Upper Cretaceous to Lower Eocene samples collected from the Nanxiong Basin are mudstones, except for sample NX9, which is siltstone. The Oligocene to recent samples taken from the Ying-Qiong Basin include sandstone, mudstone, calcareous mudstone and calcareous sandstone (Table 1). Coarse siltstones and sandstones in the Ying-Qiong Basin are chiefly subfeldspathic and feldspathic arenite, rather than quartz arenite. The detrital composition of the siltstones and sandstones in the Ying-Qiong Basin is shown in Fig. 2.

Major oxide compositions of samples from the Ying-Qiong Basin were determined at the Hubei Institute of Geology and Mineral Resources, Ministry of Land and Resources, employing wavelength X-ray fluorescence spectrometry (XRF). Loss of ignition (LOI) was determined at 980° for 90 min and FeO was determined by titration. Major oxide compositions of the samples from the Nanxiong Basin were determined at the Guangzhou Institute of Geochemistry, Chinese Academy of Sciences using XRF.

The samples from the Ying-Qiong Basin were leached with 1 N HCl to separate the residual fraction of alumino-silicates from the biogenic/authigenic fraction of carbonate, organic matter and Fe-Mn oxyhydroxides when measuring trace element and Nd isotope composition. Trace element analysis was carried out using a Perkin-Elmer Sciex ELAN 6000 ICP-MS (Perkin-Elmer, Toronto, Canada) and Nd isotope compositions were determined using a Micromass Isoprobe multi-collector inductively coupled plasma-mass spectrometer (MC-ICP-MS) at the Guangzhou Institute of Geochemistry, Chinese Academy of Sciences. Relevant analytical details are described by Liu *et al.* (1996) and Liang *et al.* (2003). The analytical precision is better than 5% for the major elements, 5–10% for trace elements and 20 p.p.m. (2σ) for Nd isotope $^{143}Nd/^{144}Nd$ ratios.

GEOCHEMISTRY

The results of major and trace elemental analyses for the Ying-Qiong and Nanxiong basins are given in Tables 1 and 2. Neodymium-isotope analyses for the Ying-Qiong Basin are shown in Table 3. To examine the geochemical characteristics of the clay from the Nanxiong Basin, enrichment factors for major and trace elements relative to PAAS (post-Archaean Australian shale, Taylor & McLennan, 1985) were determined. The enrichment factor (E_x*) for any element (x) is given by the following:

$$E_x* = \frac{C_x \text{ sample}/C_{\text{Al}} \text{ sample}}{C_x \text{ standard}/C_{\text{Al}} \text{ standard}},$$

where C_x is the concentration of the element and C_{Al} is the concentration of Al. The Al normalization is utilized because concentration of most elements (especially the immobile elements) in clay shows correlation with Al_2O_3, due to a sorting effect and absolute concentration can be disturbed by dilution (Taylor & McLennan, 1985). PAAS is used as the standard. Enrichment factor diagrams, summarized by taking average values are shown in Fig. 3.

Major elements

The SiO_2 contents of most samples from the Ying-Qiong Basin show a wide range and are consistent with the lithologies. The SiO_2 contents of sandstones are higher and range from 75 to 80 wt%. In contrast, the SiO_2 contents of mudstones are lower and range from 60 to 70 wt%. Two samples from the Meishan Formation show very low SiO_2 contents of 25–40 wt% accompanied by higher CaO. The SiO_2 contents of most samples from the Nanxiong Basin range from 50 to 70 wt% and are enriched relative to PAAS. The Al_2O_3 contents of the samples from the Ying-Qiong and Nanxiong basins are all lower than of PAAS (18·9).

The Na_2O contents of most samples from the Ying-Qiong Basin are lower and <2·0 wt%. The K_2O contents of the samples from the Oligocene Yacheng Formation to the lower part of Meishan Formation are higher and more than 3·5 wt% with the highest value at 6·34 wt%. In the sequence from the upper part of Meishan Formation to Quaternary Ledong Formation K_2O contents decrease and are <3·0 wt%. Most samples from the Nanxiong Basin show slight enrichment of Na_2O and K_2O relative to PAAS with average values of 0·96 ± 0·04 and 2·76 ± 0·54 wt%.

Table 1. X-ray fluorescence spectrometry data for the major elements (wt%) and inductively coupled plasma-mass spectrometer data for the trace elements (p.p.m.) of the samples from the Ying-Qiong Basin.

			Miocene									
	Oligocene		Lower		Middle			Upper	Pliocene			Q
No.	Q-ych	Q-lsh	Q-sya	Y-sya	Q-msh	Y-msh2	Y-msh1	Y-hl	Y-yh1	Y-yh2	Y-ygh	Y-ld
Litho	Sd	Sd	Sd	Sd	Cal-Md	Sd	Cal-Sd	Sd	Si	Md	Md	Md
Wt%												
SiO_2	81·45	76·74	83·02	78·52	27·22	78·46	36·30	76·31	74·52	65·41	64·7	65·49
TiO2	0·12	0·38	0·13	0·30	0·27	0·22	0·37	0·56	0·64	0·82	0·72	0·81
Al_2O_3	9·39	9·64	6·85	11·24	4·65	10·41	6·58	7·27	9·30	15·01	12·34	13·97
Fe_2O_3	0·27	0·01	0·95	0·47	0·64	1·40	0·50	0·19	2·11	2·65	1·06	3·25
FeO	1·28	2·30	0·90	0·82	1·10	1·25	2·67	3·40	2·45	2·75	3·50	2·60
MnO	0·02	0·03	0·03	0·02	0·04	0·01	0·04	0·10	0·04	0·06	0·05	0·07
MgO	0·24	0·23	0·16	0·29	1·47	0·25	1·44	1·22	1·37	1·90	1·78	1·95
CaO	0·13	0·98	0·58	0·41	34·9	0·22	25·60	2·43	1·93	1·74	3·43	1·22
Na_2O	1·39	0·33	1·00	1·51	0·58	1·25	0·51	1·21	1·17	1·15	1·10	1·30
K_2O	4·22	6·34	4·02	4·41	1·32	3·80	1·61	1·61	2·25	2·83	2·58	2·78
P_2O_5	0·02	0·06	0·29	0·04	0·10	0·04	0·12	0·11	0·10	0·10	0·11	0·10
H_2O^+	1·23	1·34	0·78	1·67	1·51	1·86	1·90	1·34	2·58	4·13	2·87	3·91
CO_2	0·04	0·29	0·05	0·12	26·44	0·06	22·2	4·11	1·27	1·27	5·58	0·59
Total	99·80	98·67	98·76	99·82	100·28	99·23	99·79	99·86	99·73	99·82	99·82	98·04
p.p.m.												
Sc	1·01	4·41	0·65	2·25	5·01	1·77	6·83	8·15	6·40	12·3	9·59	12·4
Ti	384	1622	436	1137	2823	784·1	3230	2790	2966	3943	5116	3996
V	4·38	29·3	9·23	19·3	40·2	14·5	72·7	47·7	48·1	82·6	71·1	77·2
Cr	13·9	15·5	6·90	5·71	41·6	8·61	65·6	64·1	39·0	68·7	64·1	79·6
Mn	12·8	36·7	43·6	22·0	30·8	17·9	23·0	13·8	56·3	73·7	20·2	92·6
Co	0·28	0·78	0·61	0·78	2·05	0·58	2·93	1·48	2·30	4·52	3·82	4·39
Ni	0·71	1·09	21·0	0·62	7·06	2·59	13·8	8·14	7·53	16·3	11·1	18·2
Ga	8·62	10·6	6·37	10·3	13·2	9·98	16·0	10·4	10·0	18·5	19·6	17·3
Ge	1·58	1·59	1·28	1·40	1·57	1·51	1·95	1·88	1·74	2·08	2·07	2·17
Rb	167	315	141	156	138	142	134	74·6	93·7	144	142	137
Sr	38·4	34·9	55·5	125	83·1	162	62·2	61·4	52·8	54·0	83·9	66·2
Y	8·47	9·57	2·03	6·11	10·6	8·89	12·6	18·2	14·8	22·7	21·0	23·2
Zr	17·2	107	39·9	76·6	253	47·0	323	311	153	229	246	293
Nb	5·33	9·14	3·14	9·58	14·6	8·19	15·9	13·7	14·7	19·3	21·3	19·2
Ba	696	925	594	716	443	492	428	140	397	455	457	792
La	10·1	19·3	4·22	12·6	21·1	22·0	25·3	33·4	33·7	39·9	42·2	39·3
Ce	19·5	37·0	6·31	21·5	37·1	38·0	44·7	66·9	64·8	73·6	84·2	72·7
Pr	2·23	4·23	0·64	2·41	4·41	4·02	5·21	7·43	7·56	8·83	9·64	8·66
Nd	8·08	15·4	2·05	8·79	15·7	14·0	19·4	27·1	28·2	32·7	36·3	31·3
Sm	1·40	2·32	0·34	1·44	2·49	2·18	3·03	4·37	4·57	5·36	5·93	4·99
Eu	0·25	0·28	0·12	0·24	0·43	0·37	0·45	0·71	0·66	0·90	1·00	0·73
Gd	1·18	1·63	0·27	1·05	1·62	1·68	1·90	3·04	3·04	3·97	4·20	3·67
Tb	0·24	0·29	0·04	0·19	0·30	0·30	0·38	0·55	0·52	0·70	0·71	0·69
Dy	1·55	1·70	0·32	1·10	1·93	1·68	2·25	3·25	2·94	4·27	3·98	4·02
Ho	0·33	0·36	0·07	0·23	0·42	0·35	0·49	0·69	0·58	0·89	0·82	0·87
Er	1·01	1·15	0·26	0·68	1·30	0·93	1·53	2·09	1·69	2·60	2·39	2·60
Tm	0·16	0·18	0·05	0·11	0·22	0·14	0·25	0·33	0·26	0·41	0·37	0·41
Yb	0·99	1·22	0·36	0·77	1·41	0·84	1·72	2·08	1·60	2·52	2·30	2·54
Lu	0·15	0·18	0·06	0·12	0·23	0·12	0·28	0·32	0·24	0·39	0·36	0·39
Hf	0·80	3·48	1·45	2·61	8·09	1·65	10·1	9·15	3·75	6·99	7·39	8·39
Ta	0·69	1·20	0·44	1·31	1·44	1·15	1·43	1·22	1·30	1·78	1·52	1·65
Pb	9·27	14·9	12·1	17·1	16·5	25·6	11·4	7·85	14·5	9·81	11·1	10·6
Th	6·56	9·17	1·79	4·86	8·71	10·2	7·47	8·81	13·1	13·3	12·6	13·8
U	1·85	2·46	1·01	2·14	3·22	0·99	3·05	2·36	2·12	3·31	2·73	3·24
La/Sc	10·0	4·37	6·46	5·60	4·20	12·4	3·70	4·09	5·26	3·26	4·40	3·16

Table 1. Continued

			Miocene									
	Oligocene		Lower		Middle			Upper	Pliocene			Q
No.	Q-ych	Q-lsh	Q-sya	Y-sya	Q-msh	Y-msh2	Y-msh1	Y-hl	Y-yh1	Y-yh2	Y-ygh	Y-ld
Litho	Sd	Sd	Sd	Sd	Cal-Md	Sd	Cal-Sd	Sd	Si	Md	Md	Md
Th/Sc	6·53	2·08	2·74	2·17	1·74	5·77	1·09	1·08	2·05	1·09	1·31	1·12
Th/Cr	0·47	0·59	0·26	0·85	0·21	1·18	0·11	0·13	0·33	0·19	0·20	0·17
Th/Co	23·9	11·7	2·92	6·22	4·24	17·5	2·55	5·97	5·71	2·96	3·29	3·15
REE	47·1	85·4	15·1	51·2	88·8	86·7	107	152	150	177	194	172
HREE	5·59	6·74	1·47	4·28	7·46	6·06	8·83	12·4	10·9	15·7	15·1	15·2
LREE	41·3	78·3	13·5	46·7	80·8	80·3	97·7	139	139	160	178	157
Eu/Eu*	0·59	0·43	1·21	0·57	0·62	0·58	0·55	0·57	0·51	0·58	0·58	0·51
$La/Yb_{(N)}$	6·60	10·2	7·42	10·5	9·63	16·9	9·51	10·4	13·6	10·2	11·9	9·98

Q, Quaternary; Litho, Lithology; Sd, sandstone; Md, Mudstone; Si, Siltstone; Cal-Md, calcareous mudstone; Cal-Sd, calcareous sandstone.

Trace elements

High field strength elements and compatible elements

Th, Y, Nb and Ta contents of the samples from the Ying-Qiong Basin show a wide range from 1·79 to 13·8 p.p.m., 2·03 to 23·2 p.p.m., 3·14 to 21·3 p.p.m. and 0·45 to 1·79 p.p.m. respectively. Most samples from the Nanxiong Basin show Th, Y, Nb and Ta contents that are enriched relative to PAAS with enrichment factors of 2·04, 1·98, 2·29 and 1·58 respectively.

The Sc, V, Cr, Co and Ni contents of the samples from the Ying-Qiong Basin show a similarly wide range, from 0·65 to 12·4 p.p.m., 4·38 to 77·2 p.p.m., 5·71 to 79·6 p.p.m., 0·28 to 4·39 p.p.m. and 0·62 to 21·0 p.p.m. respectively. The Sc, V, Cr, Co and Ni contents of the samples from the Nanxiong Basin show variable degrees of depletion relative to PAAS.

Rare earth elements

Chondrite-normalized abundances are shown in Fig. 4. Sandstones from the Ying-Qiong Basin show lower REE contents than the mudstones. Samples from the Nanxiong Basin show similar but enriched REE patterns to PAAS, except for sample NX9 which displays an abnormally high REE content, possibly due to the concentration of REE rich minerals. The bulk chemistry of sedimentary rocks can be influenced by hydraulic concentration of weathering-resistant phases such as zircon, Cr-spinel, monazite, and apatite causing irregular variations in some trace elements (Cullers *et al.*, 1979; Maas & McCulloch, 1991). For example, zircon accumulation usually causes slight enrichment in Th and heavy rare earth elements (HREEs) (Cullers, 1994). Most of the samples show $La/Yb_{(N)}$ ratios higher than PAAS (8·77) and interestingly the Eu/Eu* ratios are always more negative than PAAS (0·66) in the analysed rocks ranging from 0·5 to 0·6 (Fig. 5).

Elemental ratios

Samples analysed in this study have Th/Sc, La/Sc, Th/Cr and Th/Co ratios that are all higher than PAAS (Fig. 5). In the Nanxiong Basin these ratios show little change associated with depositional age (Late Cretaceous to Early Eocene) with values ranging from 1 to 3, 3 to 7, 0 to 0·5 and 0 to 5 respectively. However, in the Ying-Qiong Basin ratios change dramatically in the Miocene from higher values in the Yacheng Formation–lower part of Meishan Formation (highest values of 6·53, 12·42, 1·19 and 23·87) to lower values in the upper part of Meishan Formation–Ledong Formation samples (lowest values of 1·09, 3·16, 0·11 and 2·55).

Nd Isotopes

$^{143}Nd/^{144}Nd$ ratios of samples from the Ying-Qiong Basin range from 0·512071 to 0·512529 and ε_{Nd} show an abrupt change during the Miocene (Fig. 6). $^{143}Nd/^{144}Nd$ ratios of pre-13·8 Ma sedimentary rocks (Yacheng Formation to lower part of Meishan Formation) are higher ranging from 0·512258 to 0·512529 and ε_{Nd} values are typically greater than −8, with an average ε_{Nd} of −5·6 (range = −2·1 to −7·4) (Table 3). The highest value is −2·13 for the

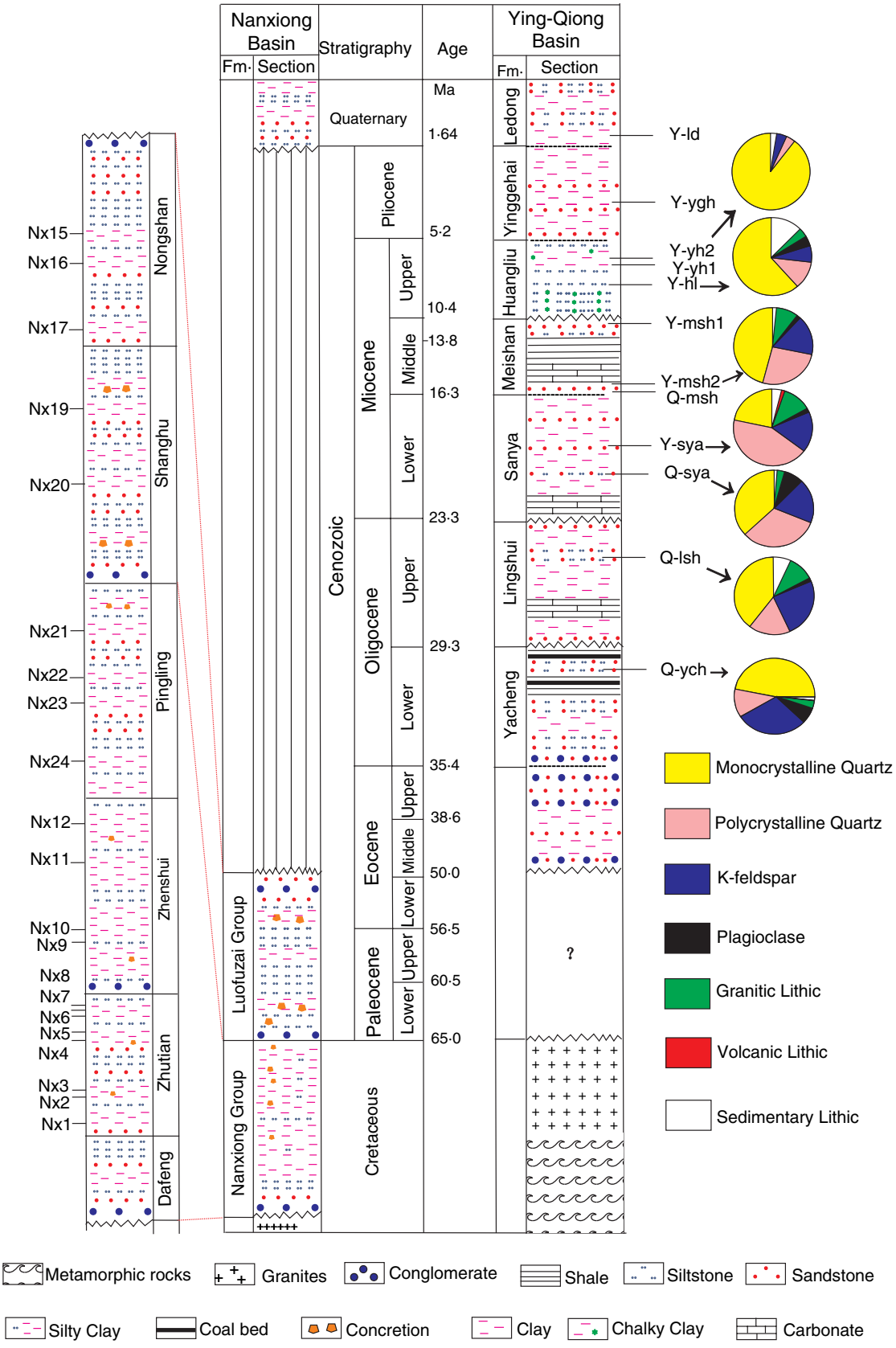

Fig. 2. General stratigraphy of the Upper Mesozoic to Cenozoic formations of the Ying-Qiong and Nanxiong basins.

Table 2. X-ray fluorescence spectrometry data for major elements (wt%) and inductively coupled plasma-mass spectrometer data for trace elements (p.p.m.) of samples from the Nanxiong Basin (post-Archaean Australian Shale from Taylor & McLennan, 1985).

	NX1	NX2	NX3	NX4	NX5	NX6	NX7	NX8	NX9	NX10	NX11
Wt%											
SiO_2	52·48	58·58	56·81	54·54	66·03	59·65	58·42	55·71	62·45	59·64	70·71
TiO2	0·64	0·58	0·65	0·68	0·53	0·70	0·74	0·73	0·65	0·59	0·59
Al_2O_3	12·36	8·78	14·16	14·98	8·00	14·70	13·35	15·48	11·58	9·34	7·75
Fe_2O_3	4·17	1·25	5·11	5·54	0·91	5·08	4·88	5·63	3·49	2·68	1·96
MnO	0·08	0·12	0·09	0·11	0·14	0·08	0·10	0·08	0·10	0·11	0·14
MgO	2·28	1·61	2·67	2·59	1·27	2·13	2·40	2·67	1·53	1·48	1·02
CaO	11·26	13·07	7·08	6·86	10·73	5·19	7·10	6·21	7·54	11·51	7·97
Na_2O	0·75	1·06	1·17	0·88	1·30	1·28	1·09	0·62	1·11	1·19	1·16
K_2O	2·85	1·66	3·17	3·67	1·35	3·31	2·97	3·81	2·55	1·83	1·48
P_2O_5	0·17	0·12	0·19	0·26	0·09	0·21	0·16	0·15	0·08	0·10	0·07
LOI	12·59	12·47	9·55	9·87	10·26	8·19	9·13	9·57	9·02	11·35	7·85
Total	99·63	99·30	100·65	99·98	100·61	100·52	100·34	100·66	100·10	99·82	100·70
p.p.m.											
Sc	10·7	6·70	12·5	14·5	–	12·5	11·9	13·9	8·75	7·06	6·13
Ti	4038	3447	3989	4355	–	4239	4538	4436	3948	3522	3769
V	121	171	77·7	99·0	–	114	74·1	83·9	55·7	79·6	46·6
Cr	41·8	24·0	113	69·3	–	64·3	59·3	152	52·9	11·2	45·1
Mn	622	863	778	867	–	606	739	596	802	848	1052
Co	10·7	7·61	14·0	14·0	–	11·6	13·6	14·1	9·74	7·51	5·94
Ni	23·3	15·7	31·3	32·3	–	26·2	26·9	32·5	20·1	12·8	13·8
Cu	58·3	56·0	34·0	36·6	–	28·9	29·9	25·2	25·8	39·4	41·1
Zn	178	56·2	107	148	–	139	97·4	100	64·7	45·6	48·6
Ga	15·3	9·81	20·0	23·0	–	19·7	18·2	20·3	14·9	11·0	9·42
Ge	1·54	1·35	1·91	2·27	–	1·88	1·85	1·89	1·87	1·36	1·57
Rb	135	79·9	177	216	–	184	154	184	130	88·8	77·9
Sr	192	198	157	154	–	117	213	159	119	209	112
Y	30·8	25·6	29·9	35·5	–	41·8	30·7	26·2	106	23·1	31·2
Zr	185	264	172	197	–	259	196	130	300	240	355
Nb	17·4	15·0	21·5	22·5	–	22·8	20·6	18·7	17·5	14·9	16·0
Cs	17·5	9·79	20·3	24·7	–	20·0	18·3	24·1	13·3	9·02	8·42
Ba	258	200	731	359	–	372	562	610	240	271	183
La	41·9	32·7	48·5	53·0	–	55·6	46·7	45·3	59·4	33·4	35·5
Ce	77·9	63·2	98·3	107	–	102	91·6	88·0	121	65·2	64·8
Pr	9·71	7·80	11·4	12·5	–	12·5	11·0	10·4	13·7	7·96	8·42
Nd	34·7	28·4	39·4	44·1	–	43·0	38·4	36·5	53·5	28·6	30·6
Sm	6·48	5·43	7·63	8·57	–	8·24	7·71	7·02	12·2	5·47	6·22
Eu	1·24	0·98	1·14	1·39	–	1·18	1·30	1·33	2·89	0·96	1·12
Gd	5·70	4·51	6·04	6·83	–	6·52	6·26	5·75	15·9	4·34	5·38
Tb	0·90	0·75	0·96	1·11	–	1·03	0·97	0·86	2·67	0·72	0·87
Dy	5·74	4·74	5·99	6·78	–	6·36	5·84	5·15	17·2	4·34	5·54
Ho	1·15	0·96	1·13	1·30	–	1·27	1·15	0·99	3·48	0·83	1·09
Er	3·12	2·68	3·12	3·68	–	3·52	3·20	2·67	9·40	2·36	3·14
Tm	0·47	0·41	0·48	0·56	–	0·53	0·48	0·40	1·31	0·36	0·49
Yb	2·86	2·56	3·03	3·39	–	3·23	3·04	2·62	8·47	2·25	3·09
Lu	0·45	0·39	0·46	0·52	–	0·50	0·46	0·38	1·27	0·36	0·47
Hf	5·07	6·76	4·81	5·28	–	6·97	5·25	2·97	8·07	6·18	9·22
Ta	1·55	1·22	2·41	2·09	–	2·20	1·71	1·46	1·46	1·19	1·27
Pb	26·4	8·86	28·6	29·4	–	31·2	27·1	28·3	22·3	16·5	15. 9
Th	16·6	14·0	24·9	27·1	–	28·1	21·9	19·1	17·4	14·2	14·1
U	6·26	13·9	7·33	7·35	–	7·63	6·28	5·98	3·13	5·83	4·72
La/Sc	3·90	4·88	3·86	3·63	–	4·43	3·92	3·26	6·79	4·72	5·79
Th/Sc	1·54	2·08	1·98	1·86	–	2·24	1·83	1·37	1·99	2·01	2·29
Th/Cr	0·39	0·58	0·21	0·39	–	0·43	0·36	0·12	0·32	1·27	0·31
Th/Co	1·55	1·83	1·77	1·93	–	2·43	1·61	1·35	1·79	1·89	2·37
$La/Yb_{(N)}$	9·49	8·28	10·4	10·1	–	11·1	9·95	11·1	4·54	9·59	7·45

Table 2. Continued

	NX1	NX2	NX3	NX4	NX5	NX6	NX7	NX8	NX9	NX10	NX11
Eu/Eu*	0·62	0·60	0·50	0·54	–	0·48	0·56	0·63	0·64	0·59	0·58
REE	192	155	227	250	–	245	218	207	322	157	166
HREE	20·4	17·0	21·2	24·1	–	22·9	21·4	18·8	59·7	15·6	20·1
LREE	170	137	205	225	–	221	195	187	260	140	145
	NX12	NX24	NX23	NX22	NX21	NX20	NX19	NX17	NX16	NX15	PAAS
Wt%											
SiO_2	58·23	61·77	58·60	56·98	53·59	70·37	66·70	52·88	51·88	56·99	62·80
TiO2	0·72	0·62	0·74	0·64	0·61	0·77	0·70	0·67	0·65	0·64	1·00
Al_2O_3	12·10	10·65	12·28	12·64	12·64	11·32	10·50	15·88	12·25	14·62	18·90
Fe_2O_3	4·15	3·16	4·21	4·22	4·25	4·22	3·70	5·61	4·32	4·98	6·50
MnO	0·07	0·07	0·07	0·07	0·07	0·03	0·03	0·04	0·07	0·05	0·11
MgO	1·80	1·48	1·89	1·97	2·13	1·57	1·37	2·86	3·05	2·64	2·20
CaO	9·28	8·91	8·58	9·23	10·78	2·77	6·30	6·77	11·14	6·17	1·30
Na_2O	0·75	1·12	0·95	0·90	0·84	0·85	1·02	0·53	0·74	0·91	1·20
K_2O	2·84	2·16	2·61	2·84	2·78	2·96	2·50	4·28	2·91	3·40	3·70
P_2O_5	0·11	0·10	0·13	0·21	0·13	0·08	0·09	0·14	0·10	0·14	0·16
LOI	10·59	9·25	9·29	9·69	11·83	5·71	7·72	9·76	13·52	9·26	–
Total	100·64	99·29	99·35	99·39	99·65	100·65	100·63	99·42	100·63	99·80	–
p.p.m.											
Sc	11·6	8·19	11·1	11·0	11·6	8·81	8·25	14·1	11·9	12·6	16
Ti	4959	4003	4820	4230	4011	4577	4413	4436	4542	4226	–
V	80·3	61·4	91·6	78·1	83·2	64·8	57·6	109	89·8	90·6	150
Cr	51·6	32·7	92·5	41·1	60·3	39·3	36·6	57·7	55·5	98·8	110
Mn	593	594	554	581	624	192	236	402	648	452	–
Co	10·9	8·39	11·4	12·0	12·8	6·86	6·03	12·2	11·6	13·1	23
Ni	25·8	16·4	32·2	22·6	30·9	16·1	14·3	31·1	33·0	36·2	55
Cu	40·7	28·9	30·1	27·2	24·6	20·4	11·3	17·3	40·3	22·3	50
Zn	82·3	58·3	124	85·2	104	38·6	38·0	98·4	114	130	85
Ga	17·2	13·4	17·2	17·1	17·3	15·1	14·6	24·3	18·9	20·5	20
Ge	1·99	1·66	2·03	1·97	1·85	6·86	12·3	3·45	2·90	2·52	–
Rb	157	117	151	155	154	367	229	384	226	223	160
Sr	167	130	131	157	167	79·1	141	124	181	116	200
Y	35·8	32·2	32·6	28·9	26·8	30·5	26·9	31·9	29·2	29·5	27
Zr	236	298	260	248	174	344	297	164	185	178	210
Nb	20·0	17·5	22·1	18·2	17·2	20·6	20·2	21·6	21·0	21·2	19
Cs	20·0	17·2	19·1	22·5	20·9	102	83·8	120	74·9	56·3	–
Ba	349	266	345	535	516	369	309	421	358	1690	650
La	45·6	39·1	46·7	41·5	38·8	39·5	38·9	46·4	43·4	43·2	38·2
Ce	90·0	74·9	90·1	80·0	74·2	76·6	72·4	90·1	83·0	83·7	79·6
Pr	10·9	9·19	11·0	9·66	9·02	9·32	9·05	11·0	10·0	10·0	8·83
Nd	39·2	31·9	38·7	34·5	31·8	33·1	32·0	40·0	35·8	36·0	33·9
Sm	7·51	5·97	7·32	6·67	6·05	6·45	6·06	7·98	6·56	7·01	5·55
Eu	1·38	1·07	1·28	1·22	1·17	1·10	0·99	1·42	1·14	1·06	1·08
Gd	6·51	5·03	6·08	5·75	5·14	5·29	5·01	6·38	5·20	5·74	4·66
Tb	1·04	0·77	0·94	0·87	0·82	0·88	0·77	0·99	0·86	0·90	0·77
Dy	6·42	4·82	5·99	5·31	5·14	5·59	4·90	5·89	5·31	5·54	4·68
Ho	1·32	0·93	1·18	1·04	0·99	1·11	1·00	1·14	1·02	1·07	0·99
Er	3·67	2·68	3·36	2·94	2·78	3·17	2·76	3·15	2·92	3·02	2·85
Tm	0·57	0·40	0·51	0·44	0·41	0·49	0·44	0·46	0·45	0·47	0·40
Yb	3·51	2·47	3·05	2·67	2·59	3·14	2·71	2·82	2·71	2·80	2·82
Lu	0·53	0·38	0·47	0·43	0·41	0·48	0·41	0·44	0·42	0·43	0·44
Hf	6·18	7·66	6·74	6·43	4·59	9·10	7·75	4·27	4·77	4·91	5
Ta	1·56	1·40	1·79	1·42	1·32	1·63	1·75	1·84	1·73	1·86	–
Pb	29·4	18·7	25·5	23·2	26·1	19·7	15·3	21·7	24·1	26·5	20
Th	18·8	16·9	20·5	17·1	16·0	17·2	16·5	21·9	19·9	20·3	14·6
U	5·37	3·65	4·44	4·11	3·61	4·77	3·48	3·47	4·03	4·16	3·1
La/Sc	3·90	4·78	4·18	3·75	3·34	4·49	4·72	3·29	3·63	3·41	2·38

Table 2. Continued

	NX12	NX24	NX23	NX22	NX21	NX20	NX19	NX17	NX16	NX15	PAAS
Th/Sc	1·60	2·06	1·84	1·54	1·38	1·96	2·00	1·55	1·67	1·60	0·91
Th/Cr	0·36	0·51	0·22	0·41	0·26	0·43	0·45	0·38	0·35	0·20	0·13
Th/Co	1·71	2·01	1·79	1·42	1·25	2·51	2·74	1·79	1·71	1·54	0·63
$La/Yb_{(N)}$	8·40	10·3	9·88	10·0	9·69	8·15	9·28	10·3	10·6	9·98	–
Eu/Eu*	0·59	0·59	0·58	0·60	0·63	0·57	0·54	0·59	0·58	0·50	–
REE	218	179	216	193	179	186	177	218	199	201	–
HREE	23·5	17·5	21·6	19·4	18·3	20·1	18·0	21·2	18·9	19·9	–
LREE	193	161	194	172	159	165	158	195	178	180	–

Table 3. Lithology and Nd isotopic compositions of samples from the Ying-Qiong Basin (the present value for CHUR reservoir is $^{143}Nd/^{144}Nd = 0{\cdot}512638$ from Hamilton *et al.*, 1983).

Stratigraphy	Sample no.	Petrography	Rb (p.p.m.)	Sm (p.p.m.)	Nd (p.p.m.)	$^{143}Nd/^{144}Nd$	2σ SE	ε_{Nd}
Pleistocene	Y-ld	Mudstone	137	4·99	31·3	0·512184	0·000011	−8·86
	Y-ygh	Mudstone	142	5·93	36·3	0·512190	0·000010	−8·74
Pliocene	Y-yh2	Mudstone	144	5·36	32·7	0·512083	0·000010	−10·8
	Y-yh1	Siltstone	93·7	4·57	28·2	0·512071	0·000010	−11·1
Upper Miocene	Y-h1	Sandstone	74·6	4·37	27·1	0·512140	0·000010	−9·71
	Y-msh1	Calcareous sandstone	134	3·03	19·4	0·512181	0·000010	−8·92
Middle Miocene	Y-msh2	Sandstone	142	2·18	14·0	0·512529	0·000012	−2·13
	Q-msh	Calcareous mudstone	138	2·49	15·7	0·512258	0·000010	−7·41
Lower Miocene	Y-sya	Sandstone	156	1·44	8·79	0·512421	0·000010	−4·24
	Q-sya	Sandstone	141	0·34	2·05	0·512263	0·000013	−7·32
Oligocene	Q-1sh	Sandstone	3156	2·32	15·4	0·512368	0·000012	−5·26
	Q-ych	Sandstone	167	1·40	8·08	0·512259	0·000012	−7·40

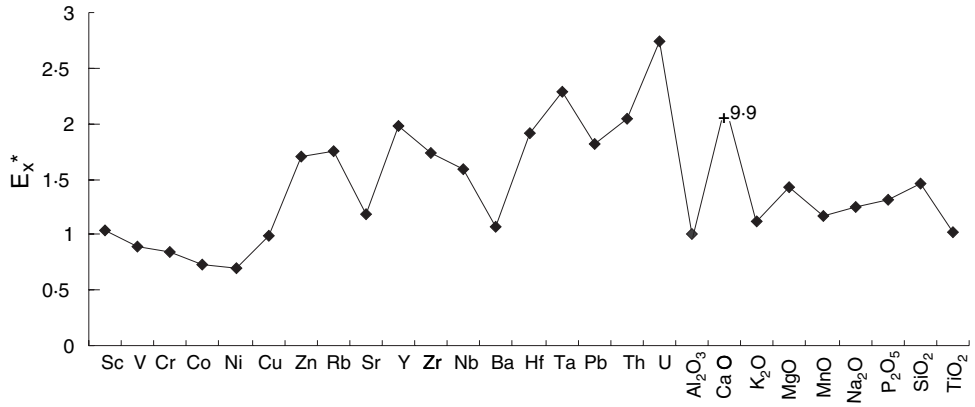

Fig. 3. Average of major and trace element enrichment factor plot (relative to post-Archaean Australian Shale, PAAS) for samples from the Nanxiong Basin (PAAS composition from Taylor & McLennan, 1985).

sample Y-msh2. In contrast, $^{143}Nd/^{144}Nd$ ratios of post-13·8 Ma (upper part of Meishan Formation to Ledong Formation) are lower ranging from 0·512071 to 0·512190 and ε_{Nd} values are less than −8, with an average ε_{Nd} of −9·3 (range = −8·7 to −11·1).

DISCUSSION

Effect of hydraulic sorting and quartz dilution

It is widely accepted that hydraulic sorting and quartz dilution can significantly influence the

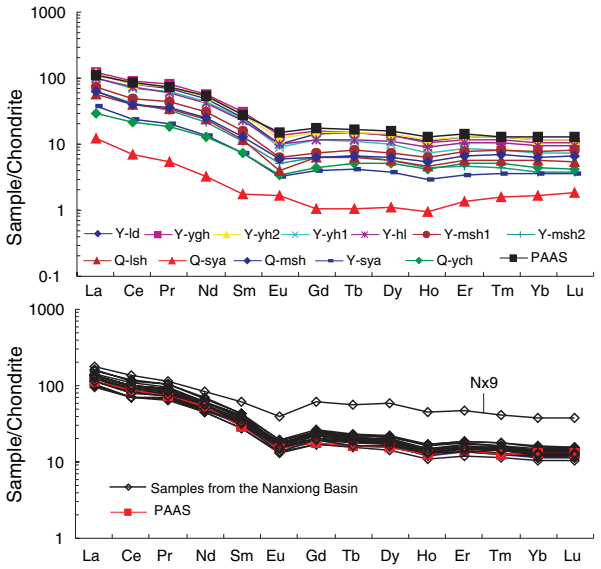

Fig. 4. Chondrite-normalized rare earth element patterns of samples from the Ying-Qiong and Nanxiong basins compared to post-Archaean Australian Shale (chondrite normalized factors from Taylor & McLennan, 1985).

chemical composition of terrigenous sediments (Cullers, 1994). Sorting and concentration of accessory minerals is especially important in the coarser rocks, with zircon, monazite and xenotime usually affecting the distribution of some trace elements (Cullers, 1994). For samples from the Nanxiong Basin, grain-size variation is limited, except sample NX9, and therefore quartz dilution should have little influence over the chemical composition of these samples. This is consistent with the poor correlations between SiO_2 and some other elements, such as SiO_2-REEs ($r = -0{\cdot}15$), SiO_2-Nb ($r = -0{\cdot}19$) and SiO_2-U ($r = -0{\cdot}13$). In contrast, samples from the Ying-Qiong Basin include mudstone, siltstone and sandstone. With this range of grain-sizes the effects of hydraulic sorting and quartz dilution may have a significant influence on chemical composition. Zircon accumulation usually causes slight enrichment in Th and HREEs, supported by the positive correlation between Zr-HREEs ($r = 0{\cdot}74$) and Zr-Th ($r = 0{\cdot}49$). Yttrium shows

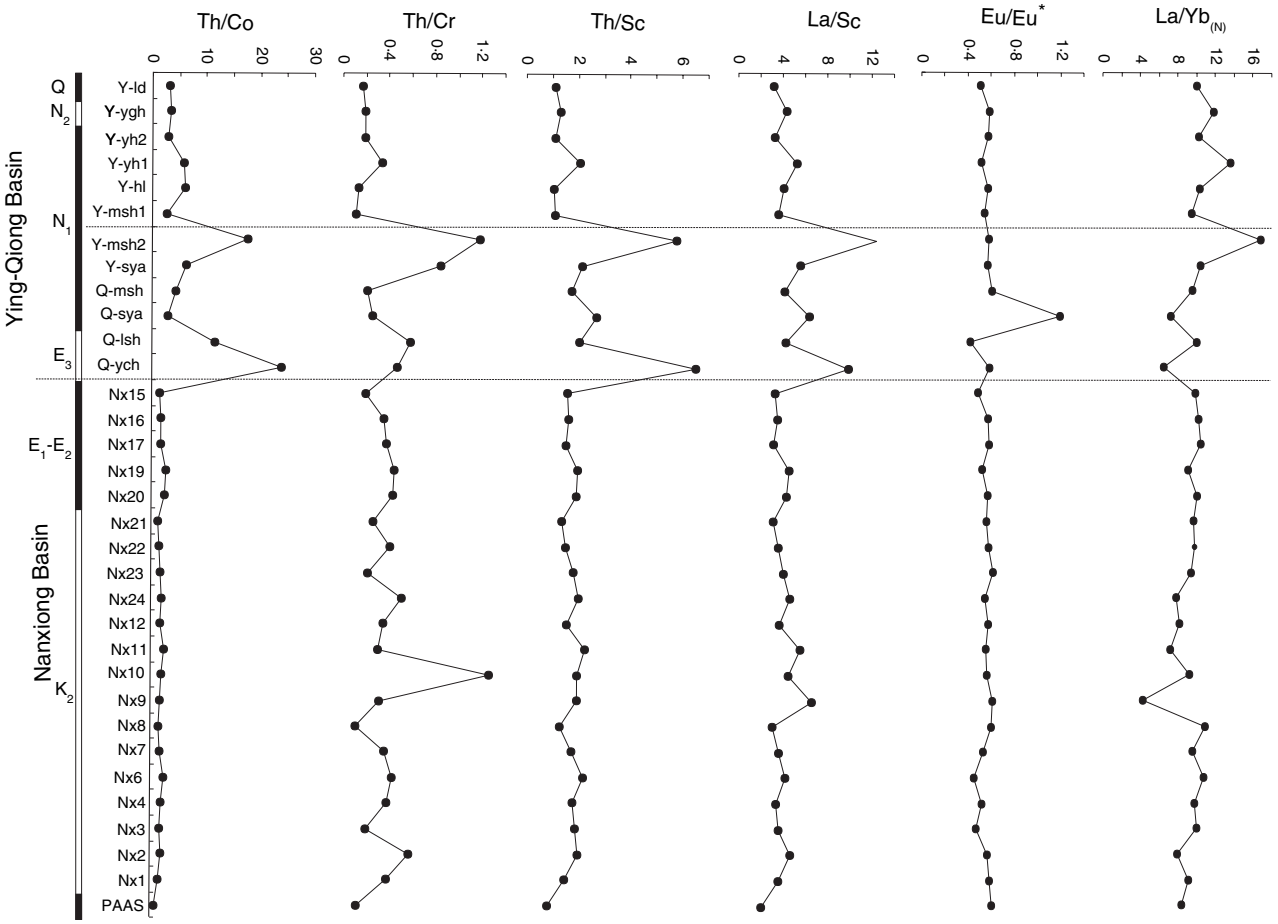

Fig. 5. Stratigraphic variation in La_N/Yb_N, Eu/Eu*, Th/Sc, La/Sc, Th/Cr and Th/Co ratios from the Ying-Qiong and the Nanxiong basins (post-Archaean Australian Shale composition from Taylor & McLennan, 1985).

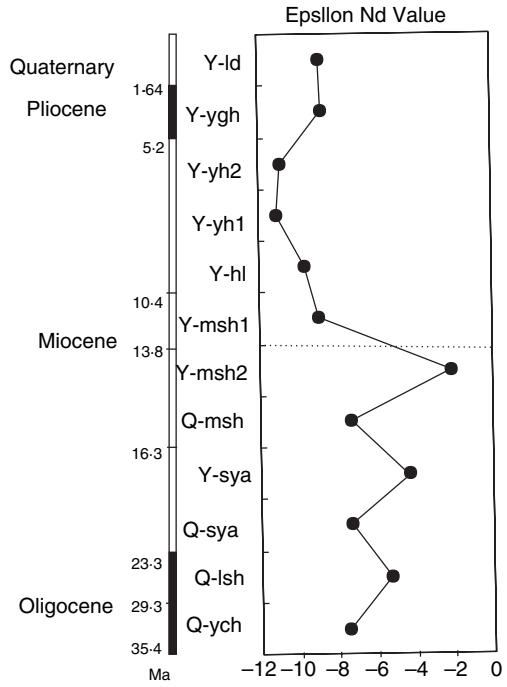

Fig. 6. Stratigraphic variation in ε_{Nd} values from the Ying-Qiong Basin.

positive correlation with LREEs ($r = 0{\cdot}96$) meaning that some phosphatic phases, such as apatite and monazite are partially controlling the REE abundances.

Studies of Nd isotopes in sediments with different grain-sizes (Revel *et al.*, 1996; Fagel *et al.*, 1997; Innocent *et al.*, 1997, 2000) show that ε_{Nd} is relatively unaffected by sedimentary processes and that any changes in ε_{Nd} linked to grain-size are due to the mixing proportions of different sediment sources (Revel *et al.*, 1996; Innocent *et al.*, 1997, 2000). The Nd results from this study come from samples with different grain-sizes. Whilst it is preferable to compare samples with the same grain-size, in many cases the mudstone and sandstone samples from this study show near to identical ε_{Nd} values on either side of the shift in average ε_{Nd} (Table 3).

Influence of marine authigenic minerals

Marine authigenic components (carbonate, organic matter and Fe-Mn oxyhydroxides) absorb dissolved Nd from the ambient sea water and therefore have Nd isotopic compositions that reflect equilibration with sea water (Wei *et al.*, 2004). Consequently, samples with a high proportion of authigenic material will have Nd isotopic compositions unrepresentative of the bulk sediment (Li *et al.*, 2003) preventing extraction of useful provenance signals.

Neodymium content in carbonates is very low, <1 μg g^{-1}, but they contain up to 200–500 μg g^{-1} in ferromanganese (Abouchami *et al.*, 1997). For this study, samples were first leached using 1 N HCl to remove the biogenic/authigenic fractions (carbonate, organic matter and Fe-Mn oxyhydroxides). A minor authigenic component (Fe-Mn oxyhydroxides), organic matter and authigenic opal may remain in the residues, but the modal abundance is usually <1% (Yoshihiro *et al.*, 1995). Moreover, the MnO contents are very low [the average value (0·04) is even lower than PAAS (0·11)] and Ce abnormal indices Ce/Ce*, an index of authigenic sediment proportion defined as $2Ce_N/(La_N + Pr_N)$, where Ce_N, La_N and Pr_N are normalized values), are all close to unity when normalized to mean continental crustal values (Fig. 7). Together, this evidence shows that any contribution from authigenic Nd must be low.

Tectonic setting, source evolution and provenance

In the discrimination diagram for sedimentary tectonic settings (Bahtia, 1983), Upper Cretaceous to Lower Eocene samples from the Nanxiong

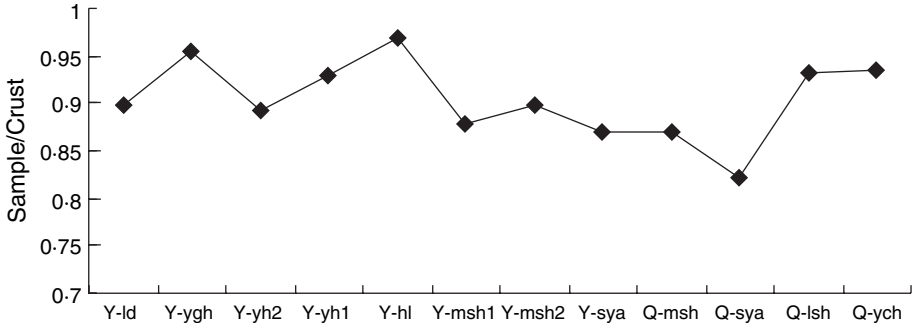

Fig. 7. Mean crust value-normalized Ce anomalies diagram for samples from the Ying-Qiong Basin (mean crust value from Taylor & McLennan, 1985).

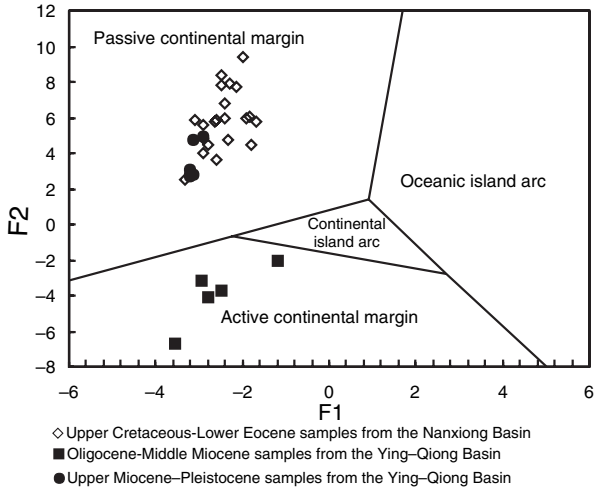

Fig. 8. Discrimination diagram for sedimentary tectonic setting for samples from the Ying-Qiong and Nanxiong basins (after Bahtia, 1983). F1 = 0·303 − 0·0447 SiO_2 − 0·972 TiO_2 + 0·008 Al_2O_3 − 0·267 Fe_2O_3 + 0·208 FeO − 3·082 MnO + 0·14 MgO + 0·195 CaO + 0·719 Na_2O − 0·032 K_2O + 7·51 P_2O_5; F2 = 43·57 − 0·421 SiO_2 + 1·988 TiO_2 − 0·526 Al_2O_3 − 0·551 Fe_2O_3 − 1·61 FeO + 2·72 MnO + 0·881 MgO − 0·907 CaO − 0·177 Na_2O − 1·84 K_2O + 7·244 P_2O_5.

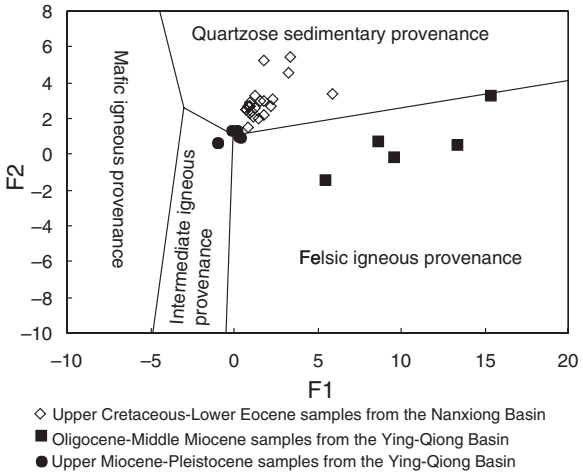

Fig. 9. Discrimination diagram for provenance of samples from the Ying-Qiong and Nanxiong basins (after Roser & Korsch, 1988). F1 = 30·638 TiO_2/Al_2O_3 − 12·541 Fe_2O_3 (total)/Al_2O_3 + 7·329 MgO/Al_2O_3 + 12·031 Na_2O/Al_2O_3 + 35·402 K_2O/Al_2O_3 − 6·382; F2 = 56·5 TiO_2/Al_2O_3 − 10·879 Fe_2O_3 (total)/Al_2O_3 + 30·875 MgO/Al_2O_3 − 5·404 Na_2O/Al_2O_3 + 11·112 K_2O/Al_2O_3 − 3·89.

Basin and Upper Miocene to Quaternary samples from the Ying-Qiong Basin plot in the passive continental margin field. In contrast, samples from the Oligocene to Middle Miocene (except sample Q-msh and Y-msh1, which show abnormally high CaO and are therefore not appropriate for discriminant diagrams) plot in the field of active continental margins (Fig. 8). In this study, CaO was corrected by 1 N HCl leaching so that any CaO from carbonate is removed. In the discrimination diagram for sedimentary provenance (Roser & Korsch, 1988), samples from the Nanxiong Basin and Upper Miocene to Pleistocene samples of the Ying-Qiong Basin plot in the quartzose sedimentary provenance, whilst samples from Oligocene to Middle Miocene of the Ying-Qiong Basin (except sample Q-msh and Y-msh1) plot in the felsic igneous provenance field (Fig. 9). This implies a major change in sediment provenance of the Ying-Qiong Basin during the Miocene, recording a switch from felsic igneous provenance field to quartzose sedimentary provenance.

Discrimination diagrams and geochemical signatures, such as Th/Sc, La/Sc, Th/Cr, Th/Co and Eu/Eu* ratios of the clays in the Nanxiong Basin have typical continental signatures and show a similar range of values across the depositional age ranging from Late Cretaceous to Early Eocene. In contrast the Oligocene to Pleistocene sedimentary rocks from the Ying-Qiong Basin, show Th/Sc, La/Sc, Th/Cr and Th/Co ratios that change considerably during the Miocene. The ratios of the Oligocene Yacheng Formation–lower part of Meishan Formation sedimentary rocks are higher than those of the upper part of Meishan Formation–Pleistocene Ledong sedimentary rocks, suggesting a higher proportion of felsic material in their source area. In addition to a marked shift in element ratios and changes in source indicated by the discrimination diagrams for sedimentary provenance and tectonic setting, the Nd isotope character also changes abruptly during the Miocene (Fig. 6).

As discussed earlier, whilst chemically immobile high field stress (HFS) element ratios of clastic sediments can be used as tracers of sediment source, the method is limited by potential effects from non-chemical processes such as hydraulic sorting. For the coarse sedimentary rocks in the Ying-Qiong Basin this might lead to a bias towards certain HFS element ratios. However, the Nd isotopic evidence is considered more robust as it appears relatively unaffected by grain-size differences (Table 3). Clift *et al.* (2002) and Li *et al.* (2003) recently reported Nd isotopic analyses for samples at ODP Site 1148, which is located on the distal passive margin of South China (Fig. 1). These Nd isotopic results are slightly different from similar age samples measured in this study, from nearby but different basins. The results reported by Clift *et al.* (2002) show a

gradual change between *ca* 23 and 16 Ma and were interpreted as representing mainly South China Block sources. In contrast, the study of Li *et al.* (2003) shows an abrupt change in Nd isotopic results between *ca* 26 and 23 Ma considered to represent a switch in source from the south-west to a northern source from *ca* 23 Ma onwards. The $^{143}Nd/^{144}Nd$ ratios reported by Clift *et al.* (2002) are *ca* 0·02–0·03% (2–3ε_{Nd} units) higher than the results reported by Li *et al.* (2003) for equivalent samples. Whereas Clift *et al.* (2002) analysed only the clay fraction (<2 μm), Li *et al.* (2003) analysed the bulk aluminosilicate fraction. Li *et al.* (2003) attributed these differences to the analysis of different sediment size fractions and the relative proportion of authigenic clay in the analysed fractions. The results from the Ying-Qiong Basin show a similar pattern to that reported by Clift *et al.* (2002) and Li *et al.* (2003), but the timing of the change is younger, at *ca* 13 Ma. Furthermore, the $^{143}Nd/^{144}Nd$ ratios measured in this study are not only higher than the bulk aluminosilicate fraction results reported by Li *et al.* (2003), but are also higher than the clay fraction results reported by Clift *et al.* (2002). The higher $^{143}Nd/^{144}Nd$ ratios measured in this study cannot be explained by analysis of different sediment size fractions. Instead it seems more probable that the data reflect a major change in sediment provenance.

The modern drainage pattern indicates that the major source of sediments at ODP Site 1148 is from within the South China Block, supplied by the Pearl River drainage system. In contrast the sedimentary rocks in the Ying-Qiong Basin are probably a mixture of South China Block and Indochina Block sources, supplied by both the Pearl River and Red River. It is likely therefore, that the differences in Nd-isotopic signatures seen in this study reflect changes in provenance linked to the Pearl River and Red River drainage systems. Robust estimate of the Nd-isotopic variation of possible sources is fundamental for the Nd isotopic provenance analysis (Li *et al.*, 2003). The Nd isotopic ratios for sediments supplied to the South China Sea are shown in Fig. 10. Similar low ε_{Nd} values are found in the Ying-Qiong Basin (upper part of Meishan to Ledong Formation), modern Mekong River and in sediments from offshore SE Indochina that indicates a dominant western provenance is present in the Ying-Qiong Basin sediments. In contrast, Oligocene to Middle Miocene sediments from the Ying-Qiong Basin show higher ε_{Nd} values than those derived from either the South China terrane or Indochina Block. Because higher ε_{Nd} values are associated with crustal blocks incorporating material more recently extracted from the mantle, there are two possible factors to explain the relatively high ε_{Nd} values seen in the Oligocene to Middle Miocene sedimentary rocks. Either there was significant addition of volcanic material or, the source region included intensive erosion of plutonic rocks with younger T_{DM}.

Addition of volcanic detritus can significantly increase the $^{143}Nd/^{144}Nd$ ratio of sediment but this scenario is unlikely: Early Cenozoic volcanism on the northern margin of the South China Sea is restricted (Chung *et al.*, 1997). Ar-Ar and K-Ar dating indicates that incipient volcanism in

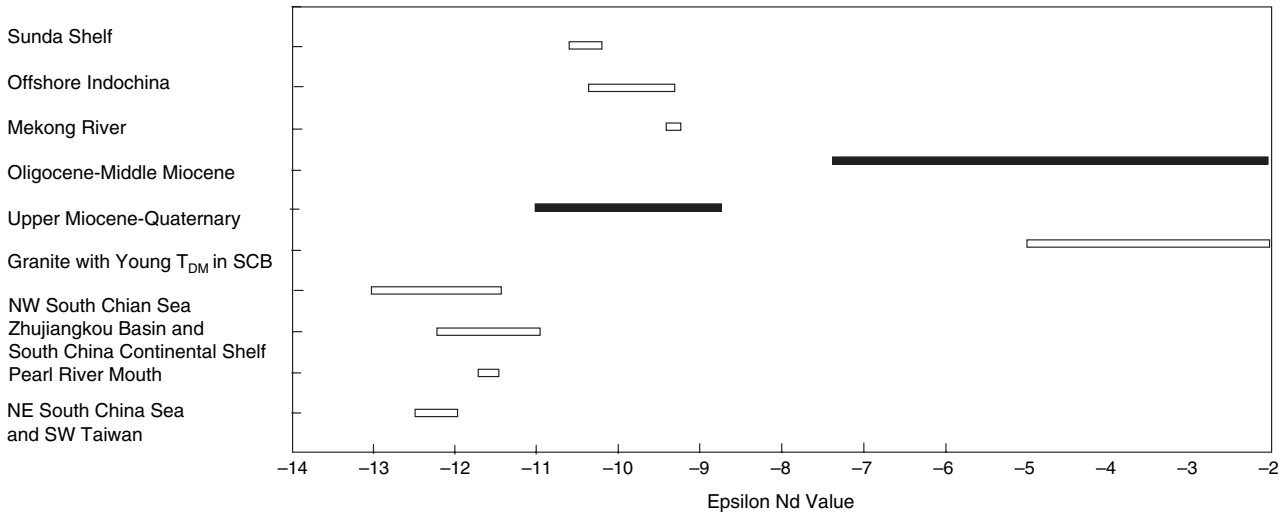

Fig. 10. Comparison of Nd values of sedimentary rocks in the Ying-Qiong Basin with possible sources surrounding the South China Sea (Chen & Jahn, 1998; Li *et al.*, 2003).

the north margin of the South China Sea occurred in the Late Oligocene and gradually increased throughout the Miocene and Pliocene (Ho *et al.*, 2000). Consequently, if addition of volcanic detritus is the main cause for the relatively high ε_{Nd} values, the Upper Miocene to Quaternary sedimentary rocks should have higher $^{143}Nd/^{144}Nd$ ratios than the Oligocene to Middle Miocene sedimentary rocks. In addition, the Oligocene to Middle Miocene sedimentary rocks have relatively high Th/Sc, La/Sc, Th/Cr and Th/Co ratios diagnostic of intermediate to silicic igneous compositions in contrast to the mostly basic–intermediate nature of the Cenozoic volcanism (Chung *et al.*, 1997). Importantly, sample petrography reveals predominantly granitic lithic material with only subordinate amounts of volcanic detritus. Samples with higher ε_{Nd} values often show higher granite lithic contents (Fig. 2). According to Chen & Jahn (1998), large areas of granite with ε_{Nd} values ranging from −2 to −5 are exposed in South China, such as Hong Kong, western Guangdong province and the south-east Guangxi province (Chen & Jahn, 1998; Fig. 10). Together, these observations show that the Nd isotopic data from Oligocene to Middle Miocene sedimentary rocks mainly reflect a major contribution of intermediate-silicic plutonic rocks with younger T_{DM}.

Tectonic controls on provenance

Changes in basin sediment provenance are related to evolution of the north margin of the South China Sea. During the Late Cretaceous to Early Eocene, numerous small rifts developed along NE-trending faults, such as the Nanxiong Basin. The Palaeozoic sedimentary cover of the South China Block was eroded and the Palaeozoic sedimentary rocks were the main basin sediment source. During the Oligocene, the centre of rifting transferred south and basins on the north margin of the South China Sea experienced rapid subsidence. Further uplift and erosion then exposed Mesozoic and Cenozoic granites that supplied large amounts of granitic detritus, especially to the Ying-Qiong Basin (Zou, 1995; Clift *et al.*, 2002). Then a change occurred at *ca* 13 Ma resulting in a reduced input from local sources (i.e. the fault blocks formed by Mesozoic-Cenozoic tectonic and magmatism) and an increasing contribution of older continental material, mostly from Indochina to the west of the South China Sea. The timing for this change coincides with a major re-organization of the sediment routing system draining south-eastern Tibet linked to uplift of the eastern Tibetan Plateau (Kirby *et al.*, 2002; Clark *et al.*, 2005) and extrusion of Indochina (Leloup *et al.*, 1995). Brookfield (1998) first suggested that the drainage of south-eastern Tibet was once very different. Clark *et al.* (2005) recently proposed that prior to the Miocene, a single river system flowed into the South China Sea through an outlet that roughly coincides with the present Red River. Then, in the Miocene (from *ca* 13 Ma), a process of surface uplift, river capture and flow reversal progressively altered the drainage system leading to the current situation where there are many large rivers with different outlets that extend from the Bay of Bengal to South China Sea (Clark *et al.*, 2005). The results of this study, recording a switch in source from local fault blocks to older continental interior rocks, mostly from the western provenance, probably reflect this major change in regional drainage. With the major re-organization of regional drainages in eastern Tibet, erosion of the older continental interior and the sediments derived from the western provenance increased since the Miocene (from *ca* 13 Ma).

CONCLUSION

Although processes such as weathering, erosion, sedimentation and diagenesis can alter the geochemical composition of basin sediments, there often remains a strong signature of the original source terrain. HFS elements can be affected by non-chemical processes (e.g. hydraulic sorting) and the ratios of REEs, Th, Sc, and high-field strength elements are less reliable indicators of provenance. In contrast Sm-Nd isotope studies have shown that the processes of weathering, transportation and deposition do not significantly alter the isotopic ratio and therefore the method is a powerful tool for investigating the sources of sedimentary rocks.

Geochemical and Nd isotopic analysis for the sedimentary rocks collected from the Nanxiong and Ying-Qiong basins show that the provenance of clastic material supplying the basins on the north margin of the South China Sea has changed in the Cenozoic. During the Late Cretaceous to Early Eocene, the Palaeozoic sedimentary cover of the South China Block was eroded and became the main basin sediment source. Further uplift and erosion then exposed Mesozoic and Cenozoic granites that supplied large amounts of granitic detritus, especially to the Ying-Qiong Basin. Then

a marked shift of Th/Sc, La/Sc, Th/Cr, Th/Co ratios and Epsilon Nd values occurred during the Miocene, at *ca* 13 Ma, recording a switch from mainly local sources (i.e. the fault blocks formed by Mesozoic-Cenozoic tectonic and magmatism) to erosion of older continental interior sources, mostly from Indochina to the west of the South China Sea. The timing for this change coincides with a major change in regional drainage driven by uplift of eastern Tibet and probably reflects this major change in regional drainage.

ACKNOWLEDGEMENTS

We thank P. Clift, J. D. Gleason and R. Cullers for their careful reviews and suggestions for improving the manuscript. This work was financially co-supported by the National Natural Science Foundation of China (no. 40306010), the Chinese Academy of Sciences (no. KZCX2-SW-117) and Key Laboratory of Marginal Sea Geology, Chinese Academy of Sciences (BYH03A06).

REFERENCES

Abouchami, W., Goldstein, S.L., Galer, S.J.G., Eisenhaucer, A. and **Mangini, A.** (1997) Secular change of lead and neodymium in central Pacific seawater recorded by a Fe-Mn crust. *Geochim. Cosmochim. Acta*, **61,** 3957–3974.

Ames, L., Zhou, G.Z. and **Xiong, B.C.** (1996) Geochronology and isotopic character of ultrahigh-metamorphism with implications for collision of the Sino-Korean and Yangtze cratons, central China. *Tectonics*, **15,** 472–489.

Bahtia, M.R. (1983) Plate tectonics and geochemical composition of sandstones. *J. Geol.*, **91,** 611–627.

Biscaye, P.E., Chesselet, R. and **Prospero, J.** (1974) Rb-Sr, $^{87}Sr/^{86}Sr$ isotope systems as an index of the provenance of continental dust in the Atlantic Ocean. *J. Rech. Atmosph.*, **8,** 819–829.

Brookfield, M.E. (1998) The evolution of the great river systems of southern Asia during the Cenozoic India-Asia collision: rivers draining southwards. *Geomorphology*, **22,** 285–312.

Chen, J.F. and **Jahn, B.M.** (1998) Crustal evolution of southeastern China: Nd and Sr isotopic evidence. *Tectonophysics*, **284,** 101–133.

Chung, S.L., Cheng, H., Jahn, B.M., Suzanne, Y.O. and **Zhu, B.Q.** (1997) Major and trace, and Sr-Nd isotope constrains on the origin of Paleogene volcanism in South China prior to the South China Sea opening. *Lithos*, **40,** 203–220.

Clark, M.K., House, M.A., Royden, L.H., Whipple, K.X., Burchfiel, B.C., Zhang, X. and **Tang, W.** (2005) Late Cenozoic uplift of Southeastern Tibet. *Geology*, **33,** 525–528.

Clauer, N. and **Chaudhuri, S.** (1992) Indirect dating of sediment-hosted ore deposists: promises and problem. In: *Isotopic Signatures and Sedimentary Records. Lecture Notes in Earth Sciences 43* (Eds N. Clauer and S. Chaudhuri), pp. 361–388. Springer.

Clift, P., Lee, J.I., Clark, M.K. and **Blusztajn, J.** (2002) Erosional response of South China to arc rifting and monsoonal strengthening: a record from the South China Sea. *Mar. Geol.*, **184,** 207–226.

Condie, K.C. (1993) Chemical composition and evolution of the upper continental crust: contrasting results from surface samples and shales. *Chem. Geol.*, **104,** 1–37.

Cullers, R.L. (1994) The controls on the major and trace element variation of shales, siltstones, and sandstones of Pennsylvanian-Permian age from uplifted continental blocks in Colorado to platform sediment in Kansas, USA. *Geochim. Cosmochim. Acta*, **58,** 4955–4972.

Cullers, R.L., Chaudhuri, S., Kilbane, N. and **Koch, R.** (1979) Rare earths in size fractions and sedimentary rocks of Pennsylvanian–Permian age from the mid-continent of the USA. *Geochim. Cosmochim. Acta*, **43,** 1285–1302.

Dewey, J.F., Cande, S. and **Pitamn, W.C.** (1989) Tectonic evolution of the India/Eurasia collision zone. *Eclogae Geol. Helv.*, **82,** 717–734.

England, P. and **Houseman, G.** (1986) Finite strain calculations of continental deformation 2. Comparison with the India-Asia collision zone. *J. Geophys. Res.*, **91,** 3664–3676.

Fagel, N., Andre, L. and **Debrabant, P.** (1997) Multiple seawater derived geochemical signatures in Indian oceanic pelagic clays. *Geochim. Cosmochim. Acta*, **61,** 989–1008.

Goldstein, S.L., O'Nions, R.K. and **Hamilton, P.J.** (1984) A Sm-Nd isotopic study of atmospheric dusts and particulates from major river systems. *Earth Planet. Sci. Lett.*, **70,** 221–236.

Gong, Z.S. and **Li, S.T.** (1997) *Continental Margin Basin Analysis and Hydrocarbon Accumulation of the Northern South China Sea*. Science Press, Beijing. pp. 124–200.

Grousset, F.E., Biscaye, P.E., Zindler, A., Prospero, J. and **Chester, R.** (1988) Neodymium isotopes as tracers in marine sediments and aerosols: North Atlantic. *Earth Planet Sci. Lett.*, **87,** 367–378.

Hamilton, P.J., O'Nions, R.K., Bridgewater, D. and **Nutman, A.P.** (1983) Sm-Nd studies of Archean metasedimentts and metavolcanics from west Greenland and their implication for the earth's early history. *Earth Planet. Sci. Lett.*, **62,** 263–272.

Ho, K.S., Chen, J.C. and **Juang, W.S.** (2000) Geochronology and geochemistry of late Cenozoic basalts from the Leiqiong area, southern China. *J. Asian Earth Sci.*, **18,** 307–324.

Houseman, G. and **England, P.** (1996) Crustal thicking versus lateral expulsion in the India-Asia collision. In: *The Tectonic Evolution of Asia* (Eds A. Yin and M. Harrison), pp. 1–17. Cambridge University Press, New York.

Innocent, C., Fagel, N., Stevenson, R.K. and **Hillaire-Marcel, C.** (1997) Sm-Nd signature of modern and late Quaternary sediments from the northwest North Atlantic: implications for deep current changes since the Late Glacial Maximum. *Earth Planet. Sci. Lett.*, **146,** 607–625.

Innocent, C., Fagel, N. and **Hillaire-Marcel, C.** (2000) Sm-Nd isotope systematics in deep-sea sediments: clay-size versus coarse fractions. *Mar. Geol.*, **168,** 79–87.

Jacobsen, S.B. (1988) Isotopic constraints on crustal growth and recycling. *Earth Planet. Sci. Lett.*, **90,** 315–329.

Kirby, E., Reiners, P.W., Krol, M.A., Whipple, K.X., Hodges, K.V., Farley, K.A., Tang, W. and **Chen, Z.** (2002) Late Cenozoic evolution of the eastern margin of the Tibetan Plateau: inferences from 40Ar/39Ar and (U-Th)/He thermochronology. *Tectonics*, **21,** 1–20.

Lacassin, R., Malushi, H. and **Leloup, P.H.** (1997) Tertiary diachronic extrusion and deformation of western Indochi-

na: structural and $^{40}Ar/^{39}Ar$ evidence from NW Thailand. *J. Geophys. Res.*, **102,** 10013–10037.

Leloup, P.H., Lacassin, R., Tapponnier, P., Schärer, U., Zhong, D.L., Liu, X.H., Zhang, L.S., Ji, S.C. and **Trinh, P.T.** (1995) The Ailao Shan-Red River shear zone (Yunnan, China), Tertiary transform boundary of Indochina. *Tectonophysics*, **251,** 3–84.

Li, X.H. and **McCulloch, M.T.** (1996) Secular variation in the Nd isotopic composition of Neoproterozoic sediments from the southern margin of the Yangtze block: evidence for a Proterozoic continental collision in southeast China. *Precambrian Res.*, **76,** 67–76.

Li, X.H., Wei, G.J., Shao, L., Liu, Y., Liang, X.R., Jian, Z.M., Sun, M. and **Wang, P.X.** (2003) Geochemical and Nd isotopic variations in sediments of the South China Sea: a response to Cenozoic tectonism in SE Asia. *Earth Planet. Sci. Lett.*, **211,** 207–220.

Liang, X.R., Wei, G.J., Li, X.H. and **Liu, Y.** (2003) Precise measurement of $^{43}Nd/^{144}Nd$ and Sm/Nd ratios using multiple-collectors inductively coupled plasma-mass spectrometer (MC-ICPMS). *Geochimica*, **32,** 91–96 (in Chinese with English abstract).

Ling, H.F., Shen, W.Z. and **Zhang, B.T.** (1996) The formation ages of the Precambrian crustal basement in Zhejiang and Fujian provinces. *Geol. Rev.*, **42,** 232–238 (in Chinese with English abstract).

Liu, Y., Liu, H.C. and **Li, X.H.** (1996) Simultaneous and precise determination of 40 trace elements in rock samples using ICP-MS. *Geochimica*, **255,** 553–558 (in Chinese with English abstract).

Maas, R. and **McCulloch, M.T.** (1991) The provenance of Archaean clastic metasediments in the Narryer gneiss complex, Western Australia: trace element geochemistry, Nd isotopes, and U-Pb ages for detrital zircons. *Geochim. Cosmochim. Acta*, **5,** 1915–1932.

McLennan, S.M. and **Taylor, S.R.** (1991) Sedimentary rocks and crustal evolution: tectonic setting and secular trend. *J. Geol.*, **99,** 1–21.

Najman, Y. and **Garzanti, E.** (2000) Reconstructing early Himalayan tectonic evolution and paleogeography from Tertiary foreland basin sedimentary rocks, northern India. *Geol. Soc. Am. Bull.*, **112,** 435–449.

Rangin, C., Klein, M., Roques, D., Pichon, X.L. and **Trong, L.V.** (1995) The Red River Fault system in the Tonkin Gulf, Vietnam. *Tectonophysics*, **243,** 209–222.

Revel, M., Cremer, M., Grousset, F.E. and **Labeyrie, L.** (1996) Grain-size and Sr-Nd isotopes as tracers of paleo-bottom current strength, Northeast Atlantic Ocean. *Mar. Geol.*, **131,** 233–249.

Roser, B.P. and **Korsch, R.J.** (1986) Determination of tectonic setting of sandstone-mudstone suites using SiO_2 content and K_2O/Na_2O ratio. *J. Geol.*, **94,** 635–650.

Roser, B.P. and **Korsch, R.J.** (1988) Provenance signatures of sandstone-mudstone suites determined using discriminant function analysis of major-element data. *Chem. Geol.*, **67,** 119–139.

Rowley, D.B. (1996) Age of initiation of collision between India and Asia: a review of stratigraphic data. *Earth Planet. Sci. Lett.*, **145,** 1–13.

Ru, K. and **Pigott, J.D.** (1986) Episodic rifiting and subsidence in the South China Sea. *AAPG Bull.*, **70,** 1136–1155.

Sun, J.Z., Li, L.B., Yang, S.G. and **Zhang, Q.M.** (1995) Evolution of transform-extension Yinggehai basin. Earth Sci.-Journal China Univ. *Geoscience*, **20,** 243–248 (in Chinese with English abstract).

Taylor, S.R. and **McLennan, S.M.** (1985) *The Continental Crust: its Composition and Evolution*. Blackwell, Oxford, 312 pp.

Wang, C., Li, X., Hu, X. and **Jansa, L.F.** (2002) Latest marine horizon north of Qomolangma (Mt Everest): implication for closure of Tethys seaway and collision tectonics. *Terra Nova*, **14,** 114–120.

Wei, G.J., Liu, Y., Li, X.H., Shao, L. and **Fang, D.Y.** (2004) Major and trace element variations of the sediments at ODP Site 1144, South China Sea, during the last 230 ka and their paleoclimate implications. *Palaeogeogr. Palaeoclimatol. Palaeoecol.*, **212,** 331–342.

Xu, Z. (1990) Mesozoic volcanism and volcanogenic iron-ore deposits in eastern China. *Geol. Soc. Am. Spec. Pap.*, **237,** 46.

Yan, P., Zhou, D. and **Liu, H.L.** (2001) A crustal structure profile across the northern continental margin of the South China Sea. *Tectonophysics*, **338,** 1–21.

Yoshihiro, A., Tsuyoshi, T., Hikari, K. and **Akira, N.** (1995) Asian continental nature of $^{87}Sr/^{86}Sr$ ratios in north central Pacific sediments. *Earth Planet. Sci. Lett.*, **133,** 105–116.

Zhou, D., Ru, K. and **Chen, H.Z.** (1995) Kinematics of Cenozoic extension on the South China Sea continental margin and its implications for the tectonic evolution of the region. *Tectonophysics*, **251,** 161–177.

Zou, H.P. (1995) On the Diwa basin system of continental margin spreading type and its genetic mechanism. *Geotecton. Metallogen.*, **19,** 303–312 (in Chinese with English abstract).

Manuscript received 11 April 2005; revision accepted 22 June 2006

